

A user's guide to PDE models for chemotaxis

Original

A user's guide to PDE models for chemotaxis / Hillen, T.; Painter, K. J.. - In: JOURNAL OF MATHEMATICAL BIOLOGY. - ISSN 0303-6812. - 58:1-2(2009), pp. 183-217. [10.1007/s00285-008-0201-3]

Availability:

This version is available at: 11583/2973885 since: 2022-12-15T14:35:49Z

Publisher:

Springer

Published

DOI:10.1007/s00285-008-0201-3

Terms of use:

This article is made available under terms and conditions as specified in the corresponding bibliographic description in the repository

Publisher copyright

(Article begins on next page)

T. Hillen · K. J. Painter

A user's guide to PDE models for chemotaxis

the date of receipt and acceptance should be inserted later

Abstract Mathematical modelling of chemotaxis (the movement of biological cells or organisms in response to chemical gradients) has developed into a large and diverse discipline, whose aspects include its mechanistic basis, the modelling of specific systems and the mathematical behaviour of the underlying equations. The Keller-Segel model of chemotaxis [44; 45] has provided a cornerstone for much of this work, its success being a consequence of its intuitive simplicity, analytical tractability and capacity to replicate key behaviour of chemotactic populations. One such property, the ability to display “auto-aggregation”, has led to its prominence as a mechanism for self-organisation of biological systems. This phenomenon has been shown to lead to finite-time blow-up under certain formulations of the model, and a large body of work has been devoted to determining when blow-up occurs or whether globally existing solutions exist. In this paper, we explore in detail a number of variations of the original Keller-Segel model. We review their formulation from a biological perspective, contrast their patterning properties, summarise key results on their analytical properties and classify their solution form. We conclude with a brief discussion and expand on some of the outstanding issues revealed as a result of this work.

1 Introduction

From microscopic bacteria through to the largest mammals, the survival of many organisms is dependent on their ability to navigate within a complex

University of Alberta, Edmonton T6G2G1, Canada, E-mail: thillen@ualberta.ca, supported by NSERC. · Department of Mathematics and Maxwell Institute for Mathematical Sciences, Heriot-Watt University, Edinburgh, EH14 4AS, UK, E-mail: painter@ma.hw.ac.uk, partially supported by NIH Grant CA113004.

environment through the detection, integration and processing of a variety of internal and external signals. This movement is crucial for many aspects of behaviour, including the location of food sources, avoidance of predators and attracting mates. The ability to migrate in response to external signals is shared by many cell populations, playing a fundamental role co-ordinating cell migration during organogenesis in embryonic development and tissue homeostasis in the adult. An acquired ability of cancer cells to migrate is believed to be a critical transitional step in the path to tumour malignancy. The directed movement of cells and organisms in response to chemical gradients, *chemotaxis*, has attracted significant interest due to its critical role in a wide range of biological phenomena (the book of Eisenbach [28] provides a detailed biological comparison between chemotactic mechanisms across different cells and organisms). In multicellular organisms, chemotaxis of cell populations plays a crucial role throughout the life cycle: sperm cells are attracted to chemical substances released from the outer coating of the egg (e.g. [33]); during embryonic development it plays a role in organising cell positioning, for example during gastrulation (see [26]) and patterning of the nervous system (e.g. Park *et al.* [85]); in the adult, it directs immune cell migration to sites of inflammation (e.g. Wu [110]) and fibroblasts into wounded regions to initiate healing. These same mechanisms are utilised during cancer growth, allowing tumour cells to invade the surrounding environment (Condeelis *et al.* [19]) or stimulate new blood vessel growth (angiogenesis) [56]. Extensive research has been conducted into the mechanistic and signalling processes regulating chemotaxis in bacteria, particularly in *E. coli* (Baker *et al.* [4]), and in the life cycle of cell slime molds such as *Dictyostelium discoideum* (Dormann and Weijer [26]). While the biochemical and physiological bases are less well understood, chemotaxis also plays a crucial role in the navigation of multicellular organisms. The nematode worm *C. elegans* undergoes chemotaxis in response to a variety of external signals (Mori *et al.* [67]) while in insects, the fruit fly *Drosophila melanogaster* navigates up gradients of attractive odours during food location (Budick and Dickinson [10]) and male moths follow pheromone gradients released by the female during mate location (Kennedy and Marsh [47]).

Theoretical and mathematical modelling of chemotaxis dates to the pioneering works of Patlak in the 1950s [86] and Keller and Segel in the 1970s [44; 45]. The review article by Horstmann [40] provides a detailed introduction into the mathematics of the Keller-Segel (KS) model for chemotaxis. In its original form this model consists of four coupled reaction-advection-diffusion equations. These can be reduced under quasi-steady-state assumptions to a model for two unknown functions u and v which will form the basis for our study in this article. The general form of the model is

$$\begin{aligned} u_t &= \nabla(k_1(u, v)\nabla u - k_2(u, v)u\nabla v) + k_3(u, v), \\ v_t &= D_v\Delta v + k_4(u, v) - k_5(u, v)v, \end{aligned} \tag{1}$$

where u denotes the cell (or organism) density on a given domain $\Omega \subset \mathbb{R}^n$ and v describes the concentration of the chemical signal. The cell dynamics derive from population kinetics and movement, the latter comprising a diffusive flux

modelling undirected (random) cell migration and an advective flux with velocity dependent on the gradient of the signal, modelling the contribution of chemotaxis. $k_1(u, v)$ describes the diffusivity of the cells (sometimes also called *motility*) while $k_2(u, v)$ is the chemotactic sensitivity; both functions may depend on the levels of u and v . k_3 describes cell growth and death while the functions k_4 and k_5 are kinetic functions that describes production and degradation of the chemical signal. A key property of the above equations is their ability to give rise to *spatial pattern formation* when the chemical signal acts as an *auto-attractant*, that is, when cells both produce and migrate up gradients of the chemical signal.

1.1 Derivation and Applications of Chemotaxis Models

Whilst a number of further approaches have been developed (for example, stochastic and discrete approaches such as those in [99; 22; 84; 64; 66; 42]), it is the deterministic Keller-Segel continuum model that has become the prevailing method for representing chemotactic behaviour in biological systems on the population level. A large amount of effort has been expended on explaining their origin from a mechanistic/microscopic description of motion. The review by Horstmann [40] considers five methods in detail and we refer to this work for further details of this significant area. Briefly, these are (i) arguments based on Fourier's law and Fick's law (e.g. Keller and Segel [45]), (ii) biased random walk approaches (e.g. Othmer and Stevens [78]), (iii) interacting particle systems (e.g. Stevens [97]), (iv) transport equations (e.g. Alt [2] or Hillen and Othmer [35]), and (v) stochastic processes (e.g. Patlak [86]). A more recent derivation from multi-phase flow modelling has been proposed by Byrne and Owen [15].

As mentioned above, Keller-Segel type equations have become widely utilised in models for chemotaxis, a result of their ability to capture key phenomena, intuitive nature and relative tractability (analytically and numerically) as compared to discrete/individual based approaches. To illustrate the breadth of this field, we describe some of those areas that have benefited from the use of KS equations, apologising to those whose works have been omitted for succinctness.

In response to starvation, the slime mold *Dictyostelium discoideum* initiates an aggregation process conducted by relay of and migration to the chemical cAMP. A number of models have been developed based on systems of equations similar to (1) that successfully capture many key features of the lifecycle (e.g. Keller and Segel [44], Höfer *et al.* [38]). Understanding bacterial pattern formation has also benefited from modelling: certain bacteria, including *E. coli* and *S. typhimurium*, can be induced to form a variety of spatial patterns when provided a suitable environment (Budrene, Woodward and co-workers [11; 12; 107]). Mathematical models indicate a chemotactic process in which cells produce an auto-attractant may underlie this patterning (Woodward, Tyson *et al.* [107; 101], see also Murray [68]). Models based on the Keller-Segel equations have also been developed to understand whether chemotaxis may underpin embryonic pattern forming processes, such as the formation

and dynamics of the *primitive streak* (an early embryonic structure that coordinates tissue movements) [81], pigmentation patterning in snakes (Murray and Myerscough [69]) and fish (Painter *et al.* [83]) and cell colonisation and neural crest migration (Landman *et al.* [54]).

Keller-Segel type models have been developed by Lauffenburger and others [57; 3] to describe the inflammatory response of leukocytes to bacterial infection and by various authors (e.g. [14; 96]) to model their migration in a Boyden-chamber. Modelling the role of chemotaxis in pathological processes is a large field: Luca *et al.* [61] considered whether the chemotactic aggregation of microglia may provide a mechanistic basis for senile plaques during progression of Alzheimer's disease, while chemotaxis has been incorporated into the modelling of a number of distinct stages of tumour growth, including the migration of invasive cancer cells (Perumpanani *et al.* [88]), tumour-induced angiogenesis (see the reviews Chaplain [16] and Mantzaris *et al.* [63]) and macrophage invasion into tumours (Owen and Sherratt [79]). Finally, we should not neglect the modelling of taxis in the context of spatial ecological processes, including "prey-taxis" (Kareiva and Odell [43] and Lee *et al.* [58]), herd grazing (Gueron and Liron [31]) and the spatial dynamics of mountain pine beetle attacks (Logan *et al.* [60]).

1.2 The Model Variations

In addition to their utilisation within models for biological systems, a large body of work has emerged on the mathematical properties of the Keller-Segel equations (1) and, in particular, on the conditions under which specialisation or variations of (1) either form a finite-time blow-up or have globally existing solutions. The majority of this work has been devoted to a special case of (1), in which the functions k_j are assumed to have linear form (see model (M1) below), a model we shall refer to as the *minimal model* following the nomenclature of Childress and Percus [18].

The minimal model has rich and interesting properties including globally existing solutions, finite time blow-up and spatial pattern formation. Detailed reviews can be found in the survey of Horstmann [40], and in the textbooks of Suzuki [98] and Perthame [87]. We shall discuss further details of these aspects in Section 2.1.

The minimal model is derived according to a limited set of conjectures and a number of variations have been described based on additional biological realism. In this paper, we systematically consider some of these variations. For obvious reasons, it is impossible to cover all variations and, as an example, the limiting case of zero diffusion in the chemical signal studied by Levine and Sleeman [59] and coworkers will not be considered here (although we will discuss this case further within the concluding discussion). A non-diffusing signal represents an immovable entity and is perhaps more appropriately an example of *haptotaxis*.

The variations are each introduced in a form that includes a single additional parameter that, under an appropriate limit, reduces the system to the minimal form. In many cases this modification regularises the problem such that solutions exist globally in time. Hence we call the corresponding parameter

for each of the extended models the *regularisation parameter*. The regularisation parameter allows us to study in detail bifurcation conditions, pattern formation and properties of the nonuniform solutions. We will not discuss certain questions such as the convergence of solutions of the variations to the minimal model in the corresponding limit case and leave this for future studies.

Below we list the ten models studied in this paper. We give explanations, motivations and literature references in Section 2.

The Minimal Model

$$\begin{aligned} u_t &= \nabla (D\nabla u - \chi u \nabla v), \\ v_t &= \nabla^2 v + u - v. \end{aligned} \quad (\text{M1})$$

Signal-Dependent Sensitivity Models

We study two versions of signal-dependent sensitivity, the “receptor” model,

$$\begin{aligned} u_t &= \nabla \left(D\nabla u - \frac{\chi u}{(1+\alpha v)^2} \nabla v \right), \\ v_t &= \nabla^2 v + u - v, \end{aligned} \quad (\text{M2a})$$

where for $\alpha \rightarrow 0$ the minimal model is obtained, and the “logistic” model

$$\begin{aligned} u_t &= \nabla \left(D\nabla u - \chi u \frac{1+\beta}{v+\beta} \nabla v \right), \\ v_t &= \nabla^2 v + u - v, \end{aligned} \quad (\text{M2b})$$

where for $\beta \rightarrow \infty$ the minimal model follows and for $\beta \rightarrow 0$ we obtain the classical form of $\chi(v) = 1/v$.

Density-Dependent Sensitivity models

We study two models with density-dependent sensitivity, the “volume-filling” model,

$$\begin{aligned} u_t &= \nabla \left(D\nabla u - \chi u \left(1 - \frac{u}{\gamma} \right) \nabla v \right), \\ v_t &= \nabla^2 v + u - v, \end{aligned} \quad (\text{M3a})$$

where the limit of $\gamma \rightarrow \infty$ leads to the minimal model, and

$$\begin{aligned} u_t &= \nabla \left(D\nabla u - \chi \frac{u}{1+\epsilon u} \nabla v \right), \\ v_t &= \nabla^2 v + u - v, \end{aligned} \quad (\text{M3b})$$

where $\epsilon \rightarrow 0$ leads to the minimal model.

The Non-Local Model

$$\begin{aligned} u_t &= \nabla \left(D\nabla u - \chi u \overset{\circ}{\nabla}_\rho v \right), \\ v_t &= \nabla^2 v + u - v, \end{aligned} \quad (\text{M4})$$

The *non-local gradient* $\overset{\circ}{\nabla}_\rho v$ is defined in Section (2.4) and chosen such that the minimal model follows for $\rho \rightarrow 0$.

The Nonlinear-Diffusion Model

$$\begin{aligned} u_t &= \nabla (Du^n \nabla u - \chi u \nabla v), \\ v_t &= \nabla^2 v + u - v, \end{aligned} \tag{M5}$$

where the minimal model corresponds to the limit of $n \rightarrow 0$.

The Nonlinear Signal Kinetics Model

$$\begin{aligned} u_t &= \nabla (D\nabla u - \chi u \nabla v), \\ v_t &= \nabla^2 v + \frac{u}{1 + \phi u} - v, \end{aligned} \tag{M6}$$

which approximates the minimal model for $\phi \rightarrow 0$.

The Nonlinear Gradient Model

$$\begin{aligned} u_t &= \nabla (D\nabla u - \chi u \mathbf{F}_c(\nabla v)), \\ v_t &= \nabla^2 v + u - v, \end{aligned} \tag{M7}$$

The vector-valued function \mathbf{F}_c is defined in Section 2.7 and chosen such that the minimal model follows for $c \rightarrow 0$.

The Cell Kinetics Model

$$\begin{aligned} u_t &= \nabla (D\nabla u - \chi u \nabla v) + ru(1 - u), \\ v_t &= \nabla^2 v + u - v, \end{aligned} \tag{M8}$$

which in the limit of zero growth, $r \rightarrow 0$, leads to the minimal model.

1.3 Outline of the Paper

In Section 2 we provide a detailed motivation for the above models, referring to relevant literature that focuses on their biological and mathematical properties. In Section 3, mathematical approaches for determining global existence are summarised. In Section 4 we perform a linear stability analysis at the homogeneous equilibrium. We show how the instability conditions depend on the additional parameter introduced in the variations (M2)–(M8). In Section 5, numerical simulations are presented to confirm theoretical findings and explore issues regarding long-time dynamics. In Section 6 we employ a classification of spikes and plateaus from Hillen [34] to investigate the form of nonhomogeneous steady state solutions. Although the analysis does not confirm our initial conjecture, namely that models with globally existing solutions “typically” have plateau solutions, our analysis does indicate that the presence of plateau solutions is a strong indicator of global existence. Finally, we shall discuss the findings and consider some outstanding issues in the field.

| Model | $D(u)$ | $A(u)$ | $B(v)$ | $C(\nabla v)$ | $f(u)$ | $g(u)$ |
|-------|--------|--------------------------------------|-----------------------------------|---|-----------|----------------------|
| (M1) | D | u | χ | ∇v | 0 | 1 |
| (M2a) | D | u | $\frac{\chi}{(1+\alpha v)^2}$ | ∇v | 0 | 1 |
| (M2b) | D | u | $\frac{\chi(\beta+1)}{(\beta+v)}$ | ∇v | 0 | 1 |
| (M3a) | D | $u\left(1 - \frac{u}{\gamma}\right)$ | χ | ∇v | 0 | 1 |
| (M3b) | D | $\frac{u}{1+\epsilon u}$ | χ | ∇v | 0 | 1 |
| (M4)* | D | u | χ | $\overset{\circ}{\nabla}_\rho v$ | 0 | 1 |
| (M5) | Du^n | u | χ | ∇v | 0 | 1 |
| (M6) | D | u | χ | ∇v | 0 | $\frac{1}{1+\phi u}$ |
| (M7) | D | u | χ | $\frac{1}{c} \tanh\left(\frac{c\nabla v}{1+c}\right)$ | 0 | 1 |
| (M8) | D | u | χ | ∇v | $ru(1-u)$ | 1 |

Table 1 Summary of the submodels and their functional forms. *For the nonlocal model the gradient, ∇v is replaced by the non-local gradient $\overset{\circ}{\nabla}_\rho v$ (see Section 2.4).

2 The Models

The models described in the following section can be summarised in the following form:

$$\begin{aligned} u_t &= \nabla(D(u)\nabla u - A(u)B(v)C(\nabla v)) + f(u), \\ v_t &= \Delta v + ug(u) - v, \end{aligned} \quad (2)$$

on the domain $\Omega \subset \mathbb{R}^n$ with prescribed initial data. Unless stated otherwise, we shall assume zero-flux boundary conditions:

$$\mathbf{n} \cdot (D(u)\nabla u - A(u)B(v)C(\nabla v)) = \mathbf{n} \cdot \nabla v = 0,$$

where \mathbf{n} is the outer unit normal to $\partial\Omega$ and $\partial\Omega$ is piecewise smooth. In the above, it is assumed that the chemical signal acts as an *auto-attractant* and thus the chemical kinetics consist of cell-dependent chemical production and linear degradation. Where applicable, cell proliferation/death is assumed to be independent of the chemical signal. The specific functional choices for $D(u)$, $A(u)$, $B(v)$, $C(\nabla v)$, $f(u)$ and $g(u)$ are given in Table 1. In the majority of the models, $C(\nabla v)$ is simply given by ∇v and we can define the *chemotactic potential* $\phi(v)$ (Biler [7]) to be the antiderivative of $B(v)$ such that

$$B(v)\nabla v = \nabla\phi(v). \quad (3)$$

2.1 (M1) Minimal Model

The minimal model has been derived through a variety of different approaches as indicated earlier. To motivate the various models, we describe its derivation as a “space-jump” process in which cell movement is modelled as the

biased random walk of a particle executing instantaneous jumps in space (see Othmer and Stevens [78]). Whilst biologically *naive*, it serves to illustrate as to how a macroscopic model for cell movement can be derived in which the macroscopic parameters (e.g. diffusion coefficient, chemotactic sensitivity) relate to specific microscopic rules. We presume that a particle executes jumps of constant length h left or right on a discrete 1-D lattice. Assuming that particles do not interact directly, we obtain a continuous-time, discrete space evolution equation for the particle density $u(x, \tau)$ at position x , time τ to be

$$\frac{\partial u(x, \tau)}{\partial \tau} = T_{x-h}^+ u(x-h, \tau) + T_{x+h}^- u(x+h, \tau) - (T_x^+ + T_x^-) u(x, \tau)$$

where T_x^\pm gives the probability per unit time for a particle at x to jump to $x \pm h$. Different classes of movement can be modelled through the choices of these functions, for example to model chemotaxis we assume cells bias their jump in response to a local spatial gradient of the chemical v :

$$T_x^\pm = a + b (v(x \pm h, \tau) - v(x, \tau)). \quad (4)$$

We substitute these into the particle evolution equation, expand the terms of the right hand side in powers of h and introduce a time scaling $\tau = \lambda t$ to obtain

$$u_t = \lambda h^2 (a u_x - 2b u v_x)_x + O(h^4).$$

Assuming that the limits $\lim_{h \rightarrow 0, \lambda \rightarrow \infty} a \lambda h^2 = D_u$ and $\lim_{h \rightarrow 0, \lambda \rightarrow \infty} 2b \lambda h^2 = \chi_u$ exist, we have

$$u_t = (D_u u_x - \chi_u u v_x)_x.$$

The extension to higher dimensions is straightforward and, after incorporating linear chemical kinetics, we obtain

$$\begin{aligned} u_t &= \nabla (D_u \nabla u - \chi_u u \nabla v), \\ v_t &= D_v \Delta v + \mu u - \delta v, \end{aligned}$$

on the domain $\Omega \subset \mathbb{R}^n$ with zero-flux boundary conditions imposed. The above equations possess a single homogeneous steady state $(u_{ss}, \frac{\mu u_{ss}}{\delta})$ where u_{ss} is determined via the initial data as $u_{ss} = \int_{\Omega} u(\mathbf{x}, 0) d\mathbf{x} / |\Omega|$.

For each of the models, nondimensionalisation techniques are employed to reduce the number of parameters and rescale the homogeneous steady state to $(u_{ss}, v_{ss}) = (1, 1)$. While the employed scaling varies slightly, the overall technique remains the same, here illustrated only with the minimal model. Choosing the following scaling/parameter groupings,

$$\begin{aligned} \mathbf{x}^* &= \sqrt{\frac{\delta}{D_v}} \mathbf{x}, \quad t^* = \delta t, \quad u^* = u / u_{ss}, \\ v^* &= \frac{\delta}{\mu u_{ss}} v, \quad D = \frac{D_u}{D_v}, \quad \chi = \frac{\chi_u \mu u_{ss}}{\delta D_v}, \end{aligned}$$

substituting into the above equations and dropping the * 's for notational simplicity yields the *minimal* chemotaxis model (M1). Note that the nondimensionalisation ensures that $\frac{1}{|\Omega|} \int_{\Omega} u(\mathbf{x}, 0) d\mathbf{x} = 1$ and the homogeneous steady state therefore is $(\bar{u}, \bar{v}) = (1, 1)$.

For (M1) on bounded domains it has been shown that the qualitative behaviour of solutions strongly depends on the space dimension. An extensive review article by Horstmann [40] concerning (M1) and related models provides greater detail, here we summarise the essentials. In one space dimension, solutions exist globally, a fact only recently proved (Osaki and Yagi [75]). For 2-D domains, global existence depends on a threshold: when the initial mass lies below the threshold solutions exist globally, while above the threshold solutions blow up in finite time. These blow-up results for the minimal model (M1) were derived in a long sequence of papers by various authors during the 1990's and early 2000's (Horstmann [40]). In the textbook by Suzuki [98] the blow-up results were extended further and the property of *quantised blow-up* was demonstrated: blow-up points each carry a fixed mass (depending on the model parameters) and the number of possible blow-up points can be determined from the given initial cell concentration. A further source of recent results are found in the chapter “Cell Motion and Chemotaxis” in the book of Perthame [87], which includes an elegant and short proof for the existence of blow-up solutions using the second spatial moment of the particle distribution. Moreover, it is shown based on [20], that the critical function space for (M1) in $\Omega \in \mathbb{R}^n$ is $L^{n/2}(\Omega)$, meaning that a threshold value θ exists such that initial conditions below threshold in the $L^{n/2}$ -norm lead to global existing solutions, whereas initial data above threshold lead to finite time blow up.

Under the biologically relevant cases for aggregation to occur, initial conditions typically lie above this threshold — hence, while the model does predict aggregation, this takes the form of a finite time blow-up. For chemotactic bacteria such as *Salmonella typhimurium* and *E. coli* or slime molds such as *Dictyostelium discoideum* (*Dd*), aggregation into swarms and mounds is only the first step in a sequence of stages. For example, aggregation of *Dd* is followed by sorting into pre-spore and pre-stalk cells, slug formation and fruiting body development (e.g. [26]). To model the stages following the aggregation it is therefore necessary to modify the model in a manner that allows pattern formation but without blow-up.

A number of modifications have been made to the minimal model that allow global existence of solutions and hence understanding of the post-aggregation stages. We term these modifications *regularisations* and we use this paper to compare and contrast some typical cases.

Each of the regularisations that follow comprises of a single alteration to one of the functional forms in equations (2), representative of additional biological realism during the formulation of the model. Of course, in any particular biological system, several or all of these assumptions may be valid, however for ease of comparison we study each case separately.

2.2 (M2) Signal-Dependent Sensitivity

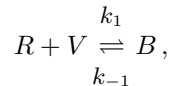
In vivo, the chemotactic response is mediated through the external detection of a signal and its subsequent transduction to internal pathways. The former will typically occur by binding of the signal to certain classes of cell surface receptors. The latter may occur either through a transformational

change of the internal receptor component or through internalisation of the entire receptor-signal complex. Once internalised, interactions with intracellular signalling pathways feeds not only into a movement response, but may also affect other pathways such as those controlling signal/receptor production and degradation. As such, the signal therefore has the potential to heavily impact on different components of the model. A common feature of many chemotaxis models is to build some of this complexity into the equations through a signal-dependent chemotactic sensitivity function. Two of the most commonly utilised forms are the “receptor” and “logistic” forms, respectively

$$k_2(u, v) = \frac{\chi}{(1 + \alpha v)^2} \quad \text{and} \quad k_2(u, v) = \frac{\chi}{v}$$

in equations (1).

The former can be motivated by a simple model for receptor-signal binding. At high concentrations of v the receptors may become fully occupied and the cell is unable to further resolve a gradient. Following the argument in [78], we let V denote a single molecule of the chemical signal, R a free cell surface receptor and B an occupied one. We take the simple reaction



and assume both that the total number of receptors is constant (i.e. there is no receptor turnover) and that the reaction is rapid. Employing a quasi steady-state hypothesis we can derive the following expression for the concentration of bound receptors

$$Phi(v) = \frac{\beta v}{\alpha v + 1}$$

where the parameters α, β depend on both the rate constants and the concentration of receptors. Here we assume that the number of bound receptors defines the chemotactic potential $\phi(v)$, that is we assume that cells base movement on a local gradient in the number of bound receptors in equation (4), rather than the local gradient of v . Then, by taking the diffusion limit and appropriate nondimensionalisation of the equations we derive the *receptor-binding* model of chemotaxis (M2a), with homogeneous steady state (1, 1). Note that the receptor-binding model formally reduces to the minimal model in the limit $\alpha \rightarrow 0$.

The above “receptor” sensitivity law has been derived and applied in numerous models for chemotaxis (e.g. Segel [93; 94], Ford *et al.* [29], Tyson *et al.* [100], Levine and Sleeman [59], [55]). By including further details of the signal transduction process, other forms of sensitivity dependence can be deduced: if co-operative binding occurs, then the concentration of bound receptors may more reasonably be described as a Hill function $\phi(v) = \frac{\beta v^n}{\alpha v^n + 1}$; the effects of internalisation of receptor-signal complexes has been incorporated by Sherratt *et al.* [96; 95]); an extension to multiple chemical species has been

investigated in Painter *et al.* [82]; memory effects have been included in a model by Boon and Herpigny [8].

We study a second form of signal-dependent sensitivity, with chemotactic potential $\phi(v) = (1 + \beta) \ln(v + \beta)$ as given by (M2b). This model can be derived using a slight variation of the biased random walk approach above (see Othmer and Stevens [78] for details) or through an argument from a ‘‘Weber-Fechner’’ law for cell behaviour [46]. Note that this model is again presented in nondimensional form with homogeneous steady state given by $(1, 1)$. With this version, we obtain the minimal model as $\beta \rightarrow \infty$, while for $\beta = 0$ we obtain the ‘‘logistic’’ chemotactic sensitivity mentioned briefly above. Although the logistic sensitivity has inherent problems, amplified on below, its prominent employment both in specific applications (e.g. [46; 21; 3; 5]) and mathematical analyses (for a review, see section 6.1.1 of Horstmann’s paper [40]) merits its consideration here. As to its problems, we note Nanjundiah [72] who writes of the logistic form ‘‘... even this fails at both, very small and very large concentrations’’ (p. 67 in [72]). By inspection, the dynamics of movement are dominated by the taxis term as $v \rightarrow 0$, whereas realistically a low signal concentration would not be expected to elicit a significant chemotactic response. This specific problem, however, can be alleviated by the form of equations given in (M2b) for $\beta > 0$.

2.3 (M3) Density-Dependent Sensitivity

Hillen and Painter ([36; 80]) introduced mechanistic descriptions of volume effects. Assuming that cells carry a certain finite (nonzero) volume and that occupation of an area limits other cells from penetrating it, a density-dependent chemotactic sensitivity function can be derived. This effect was modelled by the introduction of a function $q(u)$ describing the probability of finding space given a local cell density u . Thus, we alter equation (4) to

$$T_x^\pm = q(u(x \pm h))(a + b(v(x \pm h) - v(x))).$$

Following the derivation of the continuum limit and nondimensionalising as before, we obtain the general volume filling model

$$\begin{aligned} u_t &= \nabla \cdot (D(q - uq_u) \nabla u - \chi u q(u) \nabla v), \\ v_t &= \nabla^2 v + u - v. \end{aligned} \quad (5)$$

Our prototype volume filling model (M3a) appears for the simple and plausible choice of $q(u) = 1 - u/\gamma$, for $0 \leq u \leq \gamma$, where $\gamma \geq 1$ denotes the maximum cell density. Clearly, the volume-filling model (M3a) reduces to the minimal model as $\gamma \rightarrow \infty$, corresponding to allowing an unlimited number of cells to accumulate at each location.

The qualitative properties of the volume filling model are quite well understood. Global existence of solutions in any space dimension has been shown in [36] for (M3a) and in [109] for the full model (5) where the existence of a compact global attractor was additionally shown. The structure of the attractor can be understood using Lyapunov functions [108]. In [80] a numerical exploration was conducted to determine the longtime patterning behaviour,

revealing formation of multiple plateau type patterns which undergo a coarsening process with increasingly long transient times. In [90] the metastability of steady states was studied and the underlying bifurcation diagram was identified, revealing that the unstable eigenvalues are exponentially small. The plateau interactions were studied using asymptotic methods by Dolak and Schmeiser [25] where a system of ODEs was obtained for the location of transition layers. In [24], the volume filling idea was used to model pattern formation of *Dictyostelium discoideum* and *Salmonella typhimurium*. Burger *et al.* [13] compare two volume filling models, one with linear diffusion and the second with nonlinear diffusion of the form $\nabla(u(1-u)\nabla u)$. They prove global existence of solutions and study non-trivial steady states. Finally, Wang and Hillen [105] allow cells to squeeze into openings and include elastic cell effects through a convexity condition of $q''(u) < 0$.

An alternative form for density-dependent chemotactic sensitivity has been introduced and studied by Velazquez ([102; 103]). This model assumes that the advective velocity of cells will decrease with increasing cell density; a typical functional form for $A(u)$ that incorporates this behaviour is $A(u) = u/(1 + \epsilon u)$. Substituting this into the model and nondimensionalising the equations leads to the model (M3b). We again notice that the minimal model can be obtained in the limit $\epsilon \rightarrow 0$ and nondimensionalisation has been employed to scale the homogeneous steady state to $(1, 1)$.

2.4 (M4) Non-Local Sampling

Different cells detect spatial gradients through distinct mechanisms. Certain cells, such as *Dictyostelium discoideum*, fibroblasts and leukocytes, can detect and respond to a small gradient in the chemical signal across the length of their body using a process of internal amplification and polarisation. Smaller cells, such as *E. coli*, detect a gradient by sampling the concentration at different time points and modifying their movement accordingly. In either case, the signal detected by the cell is intrinsically *non-local* and it may therefore be appropriate to consider movement based on a *non-local gradient* by the integration of the signal by the cell over some region. A model incorporating this was postulated in [77] and a detailed derivation, analytical and numerical study has been carried out by [37].

In its nondimensional form, the *non-local* model is given by Equations (M4) with homogeneous steady state $(1, 1)$. The *non-local gradient* is defined for a constant radius $\rho > 0$ as

$$\overset{\circ}{\nabla}_{\rho} v(x, t) = \frac{n}{\omega\rho} \int_{S^{n-1}} \sigma v(x + \rho\sigma, t) d\sigma, \quad (6)$$

where $\omega = |S^{n-1}|$ and S^{n-1} denotes the $(n - 1)$ -dimensional unit sphere in \mathbb{R}^n . The nonlocal gradient describes sensing of the chemical signal over an effective sampling radius $\rho > 0$ which, in its simplest interpretation, may represent the spatial extent of the cell; effectively it provides the *dominant*

direction of the chemical signal. For example, in one spatial dimension (6) reduces to

$$\overset{\circ}{\nabla}_\rho v(x, t) = \frac{1}{2\rho} (v(x + \rho, t) - v(x - \rho, t)) .$$

Clearly, this collapses to the minimal model as $\rho \rightarrow 0$. A detailed derivation of the above model has been carried out by [37] where for $\rho > 0$ it was shown that the above equations have globally existing solutions in all space dimensions. In addition, detailed stability and numerical analyses were performed.

2.5 (M5) Nonlinear Diffusion

Typically, chemotaxis models incorporate a diffusion term into the cell dynamics to model an undirected or random component to movement. In by far the majority of applications a constant diffusion coefficient is assumed, yet it is far more likely that this term should depend nonlinearly on the signal concentration and/or the cell density, as can be seen from derivations of Keller-Segel type systems through the various approaches mentioned in the introduction (e.g. [45; 92; 96; 95; 80; 15]). An explicit example is given in the formulation of the density-dependent chemotactic sensitivity models above, where a diffusion coefficient of the form $D(u) = D(q - uq_u)$ was derived. Although the dependence on u dropped out under the special choice of $q(u) = 1 - u/\gamma$, used in the derivation of the volume-filling model (M3a), generally this would not be the case. Nonlinear dependence on the cell density has generally been neglected in studies of cell movement, yet has frequently been employed in ecological applications where it is used to describe “population-induced” movement for insect populations.

Here, we consider the case studied by Kowalczyk [50] for nonlinear diffusion of the form $D(u) = u^n$ for $n \geq 0$, i.e. the rate of diffusion increases with increasing cell density. This formulation has also been used by Eberl [27] in a model for biofilm growth. Introducing this term into our basic chemotaxis system and nondimensionalising as before leads to the *nonlinear-diffusion* model (M5), with homogeneous steady state $(1, 1)$.

As mentioned above, very few Keller-Segel based models have incorporated nonlinear dependence on the cell density in the diffusion term. Höfer *et al.* [38] introduced a phenomenological description of cell-cell adhesion in a model for *Dictyostelium discoideum* aggregation by considering $D(u) = \mu_1 + \frac{\mu_2 N^4}{N^4 + u^4}$ where N is a critical cell density. In a more theoretical study, Kuiper and Dung [52] consider nonlinear chemotaxis models with a non-linear diffusion term of the form $\nabla(P(u, v)\nabla u)$, where the nonlinear diffusion coefficient grows at least linearly in u , i.e. $P(u, v) \geq d(1 + u)$. Kuiper and Dung show that this nonlinear diffusion term dominates other typical nonlinearities and leads to global solutions and to finite dimensional attractors.

2.6 (M6) Saturating Signal Production

As remarked in Section 2.2, the binding of external signals to cell surface receptors induces a range of downstream responses that not only includes movement but also synthesis, release and degradation of the signal through interference with the appropriate pathways. These actions may be induced either by the signal itself or by other external molecules such as “quorum-sensing” cues. In either case, linear kinetics are an unduly simplistic approximation of the true signal dynamics.

Clearly, it is neither practical or illustrative to consider the many different kinetics utilised in chemotaxis models and we restrict our focus to a single form employed in a number of applications and mathematical analyses. Here, we follow example 2 in [39] and assume that the production of chemical saturates with increasing cell density; intuitively this would prevent excessive chemoattractant production as the cell density increases. Following the nondimensionalisation process, we obtain the *saturating signal production* model given by (M6) and with homogeneous steady state $(1, 1/(1 + \phi))$.

The above signalling kinetics have been used in a number of chemotactic models, for example [62; 70] and may be particularly appropriate if signal production is linked to “quorum-sensing” mechanisms.

2.7 (M7) Nonlinear Gradient Models

The chemotactic component of the general Keller-Segel model (1) is an advective term with velocity dependent on the chemical signal (Section 2.2), the cell density (Section 2.3) and the signal gradient. The linear dependence on the signal gradient (whether in local or non-local form) may allow unbounded velocities to develop, an unrealistic depiction of individual cell behaviour where cells have a maximum velocity.

A number of authors dating back to Patlak [86] in the 1950s have derived models for chemotaxis based on a more realistic description of individual cell migration (see also [2; 76]). Rivero *et al.* [92] studied a probabilistic transport equation for an individual’s migration in one dimension. Different macroscopic descriptions for a population flux were derived according to different types of migration (flagella bacteria or leukocytes). Under certain assumptions, a number of generalised Keller-Segel equations were derived in which the advective velocity $-k_2(u, v)v_x$ in Equations (1) was replaced with a form depending nonlinearly on the signal gradient, for example

$$v_0 \tanh\left(\frac{\sigma v_x}{(1 + \kappa v)^2}\right)$$

for the case of the flagella bacteria *Escherichia coli*. Notice also that their derivation resulted in a nonlinear signal-dependent diffusion coefficient.

We will therefore study a version of model (2) in which the chemotactic component to motion depends nonlinearly on the signal gradient. We base the model on that proposed in [92] for *Escherichia coli*, however, we greatly simplify their model by assuming a constant cell diffusion and a chemotactic

component that depends only on the signal gradient and a single regularisation parameter. We extend the model to a higher dimensional version, however we note that this has not been derived in detail. Following nondimensionalisation we obtain the model (M7) with homogeneous steady state $(1, 1)$. For the function $\mathbf{F}_c : \mathbb{R}^n \mapsto \mathbb{R}^n$ we shall assume

$$\mathbf{F}_c(\nabla v) = \frac{1}{c} \left(\tanh \left(\frac{cv_{x_1}}{1+c} \right), \dots, \tanh \left(\frac{cv_{x_n}}{1+c} \right) \right). \quad (7)$$

Observe that this form reduces the model to (M1) as $c \rightarrow 0$. Of course, a variety of other choices for \mathbf{F}_c may also be appropriate.

2.8 (M8) The Cell Kinetics Model

We have so far ignored the potential role of cell kinetics. This may be a reasonable modelling assumption for certain systems, for example during the aggregation stages of *Dictyostelium discoideum* when cell proliferation has halted, or if the time-scale of movement is significantly faster than that of cell growth. The inclusion of cell proliferation and cell death, however, becomes natural in systems when patterning through movement is occurring on a similar or slower timescale than that due to growth. There are many biological situations where this is likely to be the case, for example bacterial pattern formation (e.g. Tyson, Woodward *et al.* [107; 101]) or endothelial cell movement and growth in response to VEGF during angiogenesis (Chaplain and Stuart [17]).

As was the case for defining appropriate signal kinetics, the functional representation of cell growth/death will vary according to the biological system under consideration. Here we will examine a standard choice of logistic growth for the cells. Incorporating this into the minimal model and scaling the equations leads to the model (M8). Notice that this system has a single nontrivial steady state $(1, 1)$. Model (M8) has been studied numerically in [80] and interesting pattern interaction dynamics have been found. Patterns form as local maxima and complicated dynamics, which comprises merging and emerging of the maxima, subsequently occurs. An example of these dynamics is shown in (M8) of Figure 2. We will discuss the theoretical results of Osaki and Yagi [74], Wrzosek [109], and Wang and Hillen [105] in detail in the section on global existence.

A kinetic term combined with chemotaxis also appears in Wang [104], where the chemical signal is a cell nutrient and is supplied externally. Wang investigates the effects of chemotaxis and cell motility on the final population size and determines that a combination of small diffusion coefficient and large chemotaxis coefficient serve to increase the total population size.

The case for a cell kinetics term describing an Allee effect ($f(u) = u(1 - u)(u - \alpha)$) has been studied in a series of papers [65; 32; 48; 23], where it is assumed that the kinetics term acts on a faster time scale compared to that of cell movement. Depending on the choice of scaling, solutions in the form of viscous shock solutions can be found.

| Model | global existence | reference |
|-------------------|-------------------------------|--|
| (M2a) | open question | |
| (M2b) $\beta > 0$ | global existence in 2-D | Biler [7] |
| (M2b) $\beta = 0$ | global exist. below threshold | 6.1.1. in Horstmann [40] |
| (M3a) | global existence in n-D | Hillen and Painter [36] and Wrzosek [108] |
| (M3b) | global existence in n-D | Velazquez [102] and Lemma 5 |
| (M4) | global existence in n-D | Hillen, Painter, Schmeiser [37] |
| (M5) | global existence in n-D | Kowalczyk [50] |
| (M6) | global existence in n-D | Horstmann [39] |
| (M7) | global existence in n-D | Lemma 3 |
| (M8) | global existence in n-D | Wrzosek [109] |

Table 2 Summary of global existence results for the models (M2)-(M8).

3 Global Existence

Fundamental to the success of the Keller-Segel model is its ability to demonstrate aggregation in certain parameter regions, a phenomenon that can be intuitively understood through the process of chemotactic migration up gradients of a self-produced chemical. The question thus arises as to whether solutions blow-up or exist globally in time.

As mentioned earlier, the minimal model (M1) has globally existing solutions in one space dimension (Osaki and Yagi [75]) and a threshold phenomenon with blow-up solutions in higher dimensions (Horstmann [40], Suzuki [98], and Perthame [87]). For most of the modified models (M2)-(M8), global existence of solutions is known, since they have been studied theoretically or are special cases of more general models. For some of the models for which this has not previously been studied, we shall prove global existence here, while global existence of some of the models (e.g. (M2a)) remains an open problem. We summarise the relevant results in Table 2.

Exploration of the literature reveals two principal methods for demonstrating the global existence of solutions; (i) finding an L^∞ a-priori estimate for the chemotaxis term in the population flux, i.e. the term $-k_2(u, v)u\nabla v$ in (1), and (ii) to find a Lyapunov function.

The first method can be summarised in the following Lemma 1 from [37].

Lemma 1 *Let the components of the vectorfield $\Psi : \Omega \times (0, \infty) \rightarrow \mathbb{R}^n$ be uniformly bounded, and let $u_I \in L^\infty(\Omega) \cap L^1(\Omega)$ satisfy $u_I \geq 0$. Then the solution of the initial-boundary value problem*

$$u_t = \nabla \cdot (\nabla u - u\Psi), \quad u(x, 0) = u_I, \quad \mathbf{n} \cdot (\nabla u - u\Psi) = 0 \text{ on } \partial\Omega$$

satisfies $u \in L^\infty((0, \infty) \times \Omega)$ and

$$\sup_t \|u\|_\infty \leq C(\|u_I\|_1, \|u_I\|_\infty, \sup_t \|\Psi\|_\infty, n).$$

This method provides global existence for the 1-D models. A general 1-D case was studied in Osaki and Yagi [75] and applies to our models (M1), (M2a), and (M2b). Global existence for the other models is contained in the corresponding literature listed in Table 2. We summarise

Lemma 2 *Solutions to the 1D versions of models (M1)-(M8) are global in time.*

The method of uniform estimates in higher dimensions has been applied, for example, to the volume-filling model (M3a) in [36], and the non-local model (M4) in [37]. It also applies to model (M7), since the chemotaxis term contains $\Psi = \mathbf{F}_c$, with \mathbf{F}_c given in equation (7). Here Ψ is uniformly bounded and the above Lemma 1 applies directly, thus

Lemma 3 *Solutions to model (M7) exist globally in all space dimensions.*

Biler [7] derives global estimates in 2-D using the notion of *strictly sublinearity*. A chemotactic potential $\phi(v)$ is strictly sublinear, if the chemotactic sensitivity, $\chi = \phi'$ satisfies

$$\chi(v) > 0, \quad \chi(v) \rightarrow 0 \text{ as } v \rightarrow \infty \quad \text{and} \quad \chi(v)v \text{ is increasing.}$$

In this case Biler demonstrates the following result ([7]):

Lemma 4 *If $n = 2$ and $\phi(v)$ is strictly sublinear, solutions to (M2a) exist globally in time.*

This result applies to model (M2b) for $\beta > 0$.

The second method is to find a Lyapunov function. A Lyapunov function for the minimal model (M1) was simultaneously introduced by Gajewski and Zacharias [30], Biler [6] and Nagai *et al.* [71]. All authors demonstrate global existence of solutions in the sub-critical case. This Lyapunov function has inspired many further generalisations to prove global existence for chemotaxis models. Horstmann [39] developed a systematic approach to construct a Lyapunov function for cross-diffusion models. To illustrate his approach we consider a more general formulation which includes many of the above models:

$$\begin{aligned} u_t &= \nabla(D(u)\nabla u - A(u)\nabla v) \\ v_t &= \Delta v + u - v. \end{aligned} \tag{8}$$

Using Horstmann's notation from [39], we need to find a solution $R(u)$ of the differential equation

$$R''(u) = \frac{D(u)}{A(u)},$$

which satisfies $R''(u) \geq 0$. Then the functional

$$H(u, v) = \int_{\Omega} \left(\frac{v^2}{2} + \frac{|\nabla v|^2}{2} - uv + R(u) \right) dx$$

is a Lyapunov function for system (8) on a smooth domain Ω with homogeneous Neumann boundary conditions.

For the volume-filling model (M3a), $D(u) = D$ and $A(u) = \chi u(1 - \frac{u}{\gamma})$ we find

$$R_{M3a}(u) = \frac{D}{\chi} \left(u \ln u + \gamma \left(1 - \frac{u}{\gamma} \right) \ln \left(1 - \frac{u}{\gamma} \right) \right).$$

This Lyapunov function has been used by Wrzosek in [108] to prove global existence for the volume filling model.

For the model (M3b) we have $D(u) = D$ and $A(u) = \frac{\chi u}{1 + \varepsilon u}$, leading to

$$R_{M3b}(u) = \frac{D}{\chi} \left(u \ln u + \frac{\varepsilon u^2}{2} \right).$$

While Velazquez [102; 103] studied the qualitative properties of solutions to (M3b), the Lyapunov function $H(u, v)$ with R_{M3b} for (M3b) has not yet been studied in the literature. Hence we apply Horstmann's result and state

Lemma 5 *Solutions to model (M3b) exist globally in time.*

For the nonlinear diffusion model (M5) we find

$$R_{M5}(u) = \frac{D}{n(n+1)\chi} u^{n+1}.$$

This Lyapunov function has been used by Kowalczyk [50] to prove global existence.

The model (M6) was studied as Example 1 in Horstmann [39].

Table 2 reveals two cases that are not entirely solved. Model (M2a) does not fall under any of the above mentioned methods. The Lyapunov function of Horstmann cannot be constructed, and a-priori estimates of the chemotaxis term are not known. Further, the methods of Biler [7] or Post [89] do not apply.

For model (M2b) we have global existence only in 2-D and for $\beta > 0$. Biler states in [7] that strict sublinearity is not sufficient for global existence in higher dimensions ($n \geq 3$). The results for the case of $\beta = 0$ have been summarised in section 6.1.1 of Horstmann's review [40]. The results indicate that in this case there is a threshold for global existence and it has not, to our knowledge, been demonstrated whether solutions above threshold blow up in finite time.

The situation is very different for the kinetic model (M8). Here the kinetic term can control the local population growth due to migration. Our model (M8) falls into the class of models studied by Osaki *et al.* [74]. They demonstrate that certain generalisations of (M8) have global existing solutions and an exponential attractor (a compact attracting set of finite fractal dimension, that attracts bounded sets exponentially). The generalisations include choices of chemotactic potential $\phi(v) = v$, $\phi(v) = \log(1 + v)$, or $\phi(v) = \frac{v}{1+v}$.

For these choices of $\phi(v)$ we obtain the model (M8), the combined model of (M2b) and (M8), and the combined model of (M2a) and (M8), respectively. The combination of volume-filling and cell kinetic model, (M3a) and (M8) has been studied for different cases in [105] and [109], where the existence of a compact global attractor is shown in [109].

The existence and uniqueness of solutions and steady states for a related model by Chaplain and Stuart [17] has been studied by Allegretto *et al.* [1]. A global existence result for a very general cross-diffusion model with kinetic terms has been derived by Kuiper [51]. However, this model assumes no signal production, and only applies to (M8) if there is no production term in the v -equation.

4 Stability Analysis

The parameter regimes under which spatial patterning arises can be studied through a standard linear analysis at the homogeneous steady state of the models (M1)-(M8). We briefly illustrate the method using the base model (2) in one-dimension. We assume (u^*, v^*) is a spatially homogeneous steady state of (2). Linearisation about this steady state leads to the system

$$\begin{aligned} U_t &= D(u^*)U_{xx} - A(u^*)B(v^*)C'(0)V_{xx} + f'(u^*)U \\ V_t &= V_{xx} + (g(u^*) + u^*g'(u^*))U - V \end{aligned}$$

for small perturbations $U(x, t), V(x, t)$. To abbreviate the notation we will use $A^* = A(u^*), B^* = B(v^*)$, etc. The stability of the homogeneous steady state is given by the eigenvalues of the stability matrix (e.g. see Murray [68])

$$A_k = \begin{pmatrix} -k^2 D^* + f'^* & k^2 A^* B^* C'(0) \\ g^* + u^* g'^* & -k^2 - 1 \end{pmatrix}, \quad (9)$$

where $k \geq 0$ denotes the *mode*. The modes k are the eigenvalues of the Laplace operator on the given domain with the given boundary conditions. For example, on an interval $[0, L]$ with homogeneous Neumann boundary conditions we have $k = n\pi/L, n = 0, 1, 2, 3, \dots$ whilst with periodic boundary conditions we have $k = 2n\pi/L$. On the whole domain $-\infty < x < \infty$ we have $k \in \mathbb{R}_+$.

If the stability matrix A_k has eigenvalues with positive real part, then the homogeneous steady state is unstable. In that case we expect spatial pattern formation, since we know that solutions to the models (M1)-(M8) exist globally in time (Lemma 2). To study the eigenvalues of A_k we use the trace-determinant formula

$$\lambda_{1,2} = \frac{\text{tr}A_k}{2} \pm \frac{1}{2}\sqrt{(\text{tr}A_k)^2 - 4\det A_k},$$

with

$$\begin{aligned} \text{tr}A_k &= -k^2 D^* + f'^* - k^2 - 1, \\ \det A_k &= k^2 D^* (k^2 + 1) - f'^* (k^2 + 1) - (g^* + u^* g'^*) k^2 A^* B^* C'(0). \end{aligned}$$

For $f = 0$ we always have an eigenvalue $\lambda = 0$ corresponding to the mode $k = 0$. If $k \neq 0$ and $f = 0$ we see that $\text{tr}A_k < 0$, hence $\text{Re}\lambda_{1,2}$ can only be positive, if $\det A_k < 0$. Following the nondimensionalisation, each of models (M1)-(M8) have the same (nontrivial) steady state for the cell density, $u^* = 1$. Stability of the eigenvalues in each of the cases (M1)-(M8) is calculated separately (not shown here) and results are summarised in the following Lemma.

Lemma 6 *Necessary conditions for instability and the corresponding unstable modes of models (M1)-(M8) are as follows:*

(No.) necessary cond. unstable modes k
for instability

| | | |
|---------------|--|--|
| <i>(M1):</i> | $\chi > D$ | $k^2 < \frac{\chi}{D} - 1$ |
| <i>(M2):</i> | $\chi > D(1 + \alpha)^2$ | $k^2 < \frac{\chi}{D(1+\alpha)^2} - 1$ |
| <i>(M2a):</i> | $\chi > D$ | $k^2 < \frac{\chi}{D} - 1$ |
| <i>(M3a):</i> | $\chi \left(1 - \frac{1}{\gamma}\right) > D$ | $k^2 < \frac{\chi \left(1 - \frac{1}{\gamma}\right)}{D} - 1$ |
| <i>(M3b):</i> | $\chi > D(1 + \varepsilon)$ | $k^2 < \frac{\chi}{D(1+\varepsilon)} - 1$ |
| <i>(M4):</i> | $\chi > D$ | $k^2 < \frac{\chi \frac{\sin(k\rho)}{k\rho}}{D} - 1$ |
| <i>(M5):</i> | $\chi > D$ | $k^2 < \frac{\chi}{D} - 1$ |
| <i>(M6):</i> | $\chi > D(1 + \phi)^2$ | $k^2 < \frac{\chi}{D(1+\phi)^2} - 1$ |
| <i>(M7):</i> | $\chi > D(1 + c)$ | $k^2 < \frac{\chi}{D(1+c)} - 1$ |
| <i>(M8):</i> | $\chi > (\sqrt{D} + \sqrt{r})^2$ | $k^2 \in (\kappa_1, \kappa_2)$, with $\kappa_{1,2} = \frac{\chi - D - r}{2D} \pm \frac{1}{2D} \sqrt{(D + r - \chi)^2 - 4rD}$. |

It is quite clear from the above that the necessary condition for instability for each of the regularised models converges to that of the minimal model as the regularisation parameter is varied appropriately.

5 Numerical Simulations

5.1 1D Numerics

In Figure 1 (M1) we plot numerical simulations of the minimal chemotaxis model on a fixed domain $[0, 1]$ with zero-flux applied at the boundaries. The cell density and chemical concentration are plotted at distinct times, showing the growth of the 1st mode solution as cells accumulate into a sharp boundary peak.

In Figure 1 (M2)-(M8) we plot steady-state distributions for each of the regularisations as the appropriate parameter is varied. The purpose of these simulations is two-fold. Firstly we confirm the linear stability analysis through the numerical results. For zero-flux boundary conditions on the interval $[0, 1]$,

| (No.): | critical parameter value | instability for: |
|--------|--------------------------|-------------------------------|
| (M2a): | $\alpha^* = 1.144$ | $\alpha < \alpha^*$ |
| (M2b): | no critical value | $\beta \geq 0$ |
| (M3a): | $\gamma^* = 1.277$ | $\gamma > \gamma^*$ |
| (M3b): | $\varepsilon^* = 3.600$ | $\varepsilon < \varepsilon^*$ |
| (M4): | $\rho^* = 0.8127$ | $\rho < \rho^*$ |
| (M5): | no critical value | $n > 0$ |
| (M6): | $\phi^* = 1.144$ | $\phi < \phi^*$ |
| (M7): | $c^* = 3.600$ | $c < c^*$ |
| (M8): | $r^* < 3.553$ | $r < r^*$ |

Table 3 Critical parameter values for the parameters $D = 0.1$ and $\chi = 5$ on the interval $[0, 1]$ with zero-flux boundary conditions.

the smallest non-zero mode is the 1st mode, i.e. $k_c = \pi$. For each of the models (M1)–(M8) we can calculate a critical parameter using the conditions in Lemma 6, such that above (or below) this value no pattern formation is possible. Using the parameters for D and χ fixed in the numerical simulations, we list critical values in Table 3. Clearly, numerical results are consistent with the analytical results. Secondly, we consider convergence with the minimal model. For each of the models (M2)–(M7) we observe numerical convergence of solutions to the minimal model at its steady state distribution as the regularisation parameter is appropriately varied. However, the cell kinetics model (M8) does not: while solutions converge on a *short time-scale* for small values of r , over the longer time scale the kinetics term dominate and the peak density is greatly reduced.

In our next set of simulations we explore the evolution of patterns on a larger domain with random initial data, see Figure 2. We note that while the time-scale of patterning and the profile of the solutions varies from models (M1) to (M7), a consequence of the value chosen for the regularisation parameter, similar patterning dynamics are observed throughout: initially a many-peaked solution emerges which subsequently undergoes a “coarsening” process during which the wavelength increases and the number of peaks decreases. Over a longer evolution time (not shown) patterns eventually evolve into a single boundary peak pattern (for example, see [80] for numerical simulations of the volume filling model). Again, however, model (M8) demonstrates starkly different behaviour. For the chosen parameters, a continual process of coarsening and “peak renewal” occurs, in which new peaks emerge in the space between the existing ones. For other forms of cell kinetics (data not shown), solutions may eventually evolve into stable multi-peak patterns.

5.2 2-D Numerics

We next extend our numerics to consider two dimensions. Analytically the 2-D case is critical: in the biologically relevant parameter region for aggregation

to occur the minimal model displays finite-time blow up. A summary of the global existence results for the various models (M2)–(M8) was given in Section 3.

Numerical simulations on the unit square are plotted in Figure 3. For the minimal model, solutions quickly evolve into a blow-up. Following a critical time, which we classify as numerical blow-up, we are unable to track the solution any further, therefore a plot of the cell density is shown just prior to this point in the appropriate plot of Figure 3 (a).

Results from the numerical simulations of models (M2)–(M8) are displayed in the remaining plots of Figure 3 (a). The result for both forms of (M2) are somewhat ambiguous: for the model (M2a) (“receptor”) a steady state distribution in the cell density is achieved, yet the aggregation is highly concentrated and we should query as to whether the numerical scheme is sufficiently accurate at such steep gradients. A similar ambiguity appears for model (M2b) (“logistic”); whilst global existence has been proved by Biler [7] for $\beta > 0$, whereas for $\beta = 0$ global existence has only been determined below a threshold (see 6.1.1 in Horstmann [40]). The numerical results here, for $\beta = 0$ and above the threshold in [40], lead to numerical blow-up at time $t = 1.13$. To fully resolve the nature of these solutions it will be necessary to develop more sophisticated numerical schemes, for example an adaptive-meshing algorithm similar to that developed by Budd *et al.* [9]. The remaining cases, (M3)–(M8), are less ambiguous and the models have globally existing solutions. The temporal evolution of the cell density at the aggregation peak is tracked in Figure 3 (b). Two cases deserve special attention. Firstly, for the nonlinear diffusion model (M5), the cell density aggregate appears to form a compact mass with steep fronts. Secondly, for the cell kinetics model (M8), solutions initially lie close to those of the minimal model before cell kinetics dominate and the peak density drops to a steady state profile.

In our second set of 2-D numerics, we consider the evolution on a larger domain with random initial data. We split our study into two distinct cases: in the first we incorporate all of the regularisations (M2a), (M3a), (M5) and (M6) into a single model. The resulting numerics, Figure 4 (a), demonstrate the initial emergence of multiple peaks, which subsequently merge and the average wavelength increases: eventually a single boundary peak will remain. The same type of behaviour is observed when each of the regularisations is considered separately. In the second simulation we add a logistic growth term to the model of Figure 4 (a). The resulting numerical simulations demonstrate a continual process of peak collision and peak emergence, Figure 4 (b), akin to the 1-D findings. Here the average wavelength between peaks roughly remains the same.

5.3 3-D Numerics

The properties for the various models in higher dimensions are less well understood. Due to the computationally exhaustive nature of 3D simulations we restrict our numerical exploration to just 2 cases: the minimal model (M1), for which finite time blow-up occurs in 3D, and the volume-filling model (M3a), which is known to have globally existing solutions [36; 109].

As expected, 3D numerical simulations of the minimal model (not shown) demonstrate a rapid evolution to a blow-up. For the volume-filling model, however, solutions evolve into a stable spherical aggregation of cells, Figure 5 (a) from initial conditions on a small domain with biased initial data. For random initial data on a larger domain, a number of aggregates form which undergo the same coarsening process as observed above in the 1-D and 2-D numerics. A snapshot from this process is shown in Figure 5 (b).

6 Plateaus and Spikes

The various models above each show pattern formation in certain parameter ranges. Numerically these may appear either as sharp peaks (e.g. for the minimal model (M1)) or as wide plateaus (e.g. for the volume filling model (M3a)), or as combinations of these. In Hillen [34] a classification of “spikes” versus “plateaus” was formulated as:

Theorem 1 *Assume $f \in C^5(U)$ and $\text{Hess}(\Delta f(\bar{x}))$ is invertible. Then*

$$\bar{x} \text{ is a spike} \iff \text{Hess}(\Delta f(\bar{x})) \text{ is positive definite,}$$

$$\bar{x} \text{ is a plateau} \iff \text{Hess}(\Delta f(\bar{x})) \text{ is negative definite.}$$

In this section, we employ this classification in one space dimension to study the form of nontrivial steady states. Spikes and plateaus have differing stability properties (see [34]), with spikes often unstable and indicative of singular behaviour. Plateaus are often stable or metastable. Following the arguments in [34] it may be conjectured that spikes relate to models that blow-up in higher dimensions (such as the minimal model (M1)), whereas plateaus indicate global existence of solutions in any space dimension (such as for the volume-filling model (M3a)). As our analysis below demonstrates, this relation does not hold and in fact spike patterns occur for the majority of the regularised models. Numerically, plateaus have only been observed in certain parameter regions for the volume-filling (M3a) and for the nonlinear diffusion model (M5): solutions of plateau-type are labelled with an asterisk in Figure 1.

In one dimension, the criterion for spikes versus plateaus from Theorem 1 can be simplified to

Corollary 1 *Assume \bar{x} is an isolated maximum of $f(x)$ and $f \in C^5$. Then \bar{x} is a spike if and only if $f^{IV}(\bar{x}) > 0$ and \bar{x} is a plateau if and only if $f^{IV}(\bar{x}) < 0$.*

For each of the models we assume that the instability conditions of Lemma 6 are satisfied, such that the homogeneous steady state is unstable and a pattern arises. Under these assumptions we consider a steady state with isolated local maximum at \bar{x} . For this maximum we evaluate the fourth order derivatives, $u^{IV}(\bar{x}), v^{IV}(\bar{x})$. We omit the elementary details and summarise the results:

Theorem 2 *Assume the instability conditions of Lemma 6 and assume that \bar{x} is a common local maximum of a steady state $u(x), v(x)$. We denote the values at maximum by $\bar{u} = u(\bar{x}), \bar{v} = v(\bar{x})$.*

(M1): \bar{u} and \bar{v} are spikes.

(M2a): If $\bar{u} > \frac{D}{\chi}(1 + \alpha\bar{v})^2$ and $\bar{v} < \frac{\chi - 2D\alpha}{2D\alpha^2}$ then \bar{u} and \bar{v} are spikes.

(M2b): If $\bar{u} > \frac{D(\beta + \bar{v})}{\chi(\beta + 1)}$ then \bar{u} and \bar{v} are spikes.

(M3a): (see also [34]) We define

$$u_{1,2} = \frac{\gamma}{2} \left(1 \pm \sqrt{1 - \frac{4D}{\chi\gamma}} \right).$$

(i) The maxima \bar{u} and \bar{v} are plateaus if

$$u(\bar{x}) > \begin{cases} u_2 & \text{for } 4D < \chi\gamma \\ \frac{\gamma}{2} & \text{otherwise.} \end{cases}$$

(ii) If $4D < \chi\gamma$ and $\bar{u} \in (u_1, u_2)$, then \bar{u} and \bar{v} are spikes.

(M3b): If $\bar{u} > \frac{D}{\chi - \varepsilon D}$ then \bar{u} and \bar{v} are spikes.

(M4): The maximum \bar{v} is a spike. The maximum \bar{u} cannot be classified, because of the nonlocal gradient term in the equation for u .

(M5):

(i) For $n = 0$ we obtain the result for the minimal model from (M1).

(ii) For $0 < n < 1$ and $\bar{u} > \sqrt[n]{\frac{D}{\chi}}$ we obtain spikes for \bar{u} and \bar{v} .

(iii) For $n = 1$ we obtain spikes for \bar{u} and \bar{v} .

(iv) For $n > 1$ we obtain plateaus when $\bar{u} > \sqrt[n]{\frac{\chi}{D}}$. If $\bar{u} < \sqrt[n]{\frac{\chi}{D}}$ then \bar{v} is a spike.

(M6): If $\frac{\bar{u}}{(1 + \phi\bar{u})^2} > \frac{D}{\chi}$ then \bar{u} and \bar{v} are spikes.

(M7): The maximum \bar{u} cannot be classified, and \bar{v} is a spike.

(M8): If $\bar{u} > \frac{D}{\chi}(1 + r)$ then \bar{u} and \bar{v} are spikes.

Remarks:

1. The above regularisations have one additional parameter compared to the minimal model (M1). Note that taking the appropriate limit in all of the above cases shows that the conditions for spikes and plateaus match with those for the minimal model.
2. The simulations in Figure 2 confirm the theoretical result. Plateaus are marked with an asterisk *.
3. Notice that in [37] we claimed that \bar{v} is a plateau for model (M4). Unfortunately, our proof of Theorem 3 in [37] is wrong, and we use an appendix A of this paper to correct this.

7 Discussion

In this article we have explored the relevance of the Keller-Segel equations in the modelling of chemotactic cell migration. Motivated by a consideration of the different biological factors underpinning the modelling, we have systematically derived a number of variations that have received significant scrutiny in the modelling and mathematical literature. We have proceeded to summarise results pertaining to the existence of solutions to the models, their ability to initiate spatial patterning, the long-time behaviour of solutions and the form of steady state patterns.

Whilst we have made every effort to explore the consequences of a diverse set of biological assumptions, we make no claim that our analysis is complete. Indeed, there are a number of further cases that would merit consideration. For example, in the model (M5), the nonlinear diffusion depended only on the cell density; realistically this term would also depend on the signal concentration, as indicated by derivations of Keller-Segel models from microscopic descriptions of cell motion. Incorporating further details of the internal transduction of the chemical signal, the role of multiple chemical species, the effect of time delays between signal detection and response, may all lead to significantly different models compared to those considered here. Furthermore, it should be noted that in the application to a specific biological system, a combination of the models mentioned here may be appropriate. The choice as to what should be included and what can justifiably be neglected is entirely dependent on the biological system under consideration.

We have not discussed the case of zero diffusion in the chemical signal, as may occur if the signal becomes bound to a rigid external structure such as the extracellular matrix. This has been considered mathematically by Levine and Sleeman [59] and Rascle and Ziti [91] amongst others. The strong regularising property arising through signal diffusion is lost and more singular behaviour can be expected. Indeed, both Rascle and Ziti [91] and Levine and Sleeman [59] showed the existence of finite time blow-up solutions. The complimentary case of zero cell diffusion was studied by Dolak and Schmeiser [25] and Wang and Hillen [106]. In both papers it was shown that for different models shock solutions can develop.

We note that this paper has principally concentrated on the pattern forming abilities of the chemotactic equations, specifically the initiation of patterning, the dynamics of solutions and questions regarding global existence. A significant proportion of the mathematical and modelling literature has focused on other types of behaviour observed in the Keller-Segel equations, such as their ability to generate travelling wave solutions (e.g. [46; 73; 41; 53]).

From a mathematical point of view, a number of open problems are revealed as a result of the explorations here. It would be of significance to study in detail the convergence to the minimal model under the corresponding parameter limit of models (M2)-(M8). In particular, in 2-D solutions to all the models must become unbounded. To our knowledge this has so far only been investigated for model (M3b) by Velazquez [102; 103]. Of particular interest here is the question of convergence for model (M8): while numerical simulations in 1D demonstrated a close similarity at the heterogeneous steady states for

models (M2)-(M7) as the regularisation parameter was varied appropriately (Figure 1, top row), this did not occur in the case (M8) – convergence only occurred on a short time scale before the kinetic term begins to dominate. Another interesting limit occurs for model (M2b) as $\beta \rightarrow 0$. As mentioned earlier, the singular case of $\chi = 1/v$ is not so relevant biologically, but it has been studied mathematically in many publications. It would be of interest to observe whether the singularity produces effects not observed in the regularised cases of $\beta > 0$.

A complete understanding of global existence is still lacking. For example, global existence of model (M2a), one of the more widely utilised forms of chemotactic sensitivity, remains open. A complete classification of global existence/blow-up in model (M2b) for the case $\beta = 0$ is also absent.

Penetration into the long-time dynamics of solutions requires significant further analysis. Numerical simulations of the models typically reveal merging of local maxima. These dynamics have so far been studied for the volume filling model (M3a) by Potapov and Hillen [90] and by Dolak and Schmeiser [25]. For the other models this has not been done, however, merging dynamics are also known from other cross-diffusion models. For example, merging dynamics for the Brusselator model has been studied by T. Kolokolnikov [49], and it is believed the instability for the chemotaxis models might well be of the same type (personal communication). Of further interest are the merging and emerging dynamics observed in the kinetics model (M8). We are currently pursuing some first ideas to tackle these problems.

A Correction of an earlier classification of plateaus for (M4)

The original definition of spikes versus plateaus as given in [34] is based on the non-local gradient $\overset{\circ}{\nabla}_\rho$. In one dimension, a maximum $f(\bar{x})$ is defined to be a spike, if there exists an $\rho^* > 0$ such that $0 > \overset{\circ}{\nabla}_\rho f'(\bar{x}) > f''(\bar{x})$ for each $0 < \rho < \rho^*$, and a plateau, if there exists a $\rho^* > 0$ such that $0 > f''(\bar{x}) > \overset{\circ}{\nabla}_\rho f'(\bar{x})$ for each $0 < \rho < \rho^*$. Hence Corollary 1 is an equivalent formulation for smooth functions.

In [37] it has been claimed for model (M4) that \bar{v} is a plateau. Unfortunately, the proof of Theorem 3 in [37] is wrong, since the function $\psi = u \exp(-\chi v)$ typically has a minimum at \bar{x} , and not a maximum, as assumed in [37]. We use this opportunity to correct the proof and show that typically, \bar{u} and \bar{v} are spikes.

For the steady state equations of (M4) we compute for an isolated maximum \bar{x} that

$$\bar{v}'' = \bar{v} - \bar{u} \tag{10}$$

$$\bar{u}'' = \frac{\chi \bar{u}}{D} \overset{\circ}{\nabla}_\rho \bar{v}' \tag{11}$$

$$\bar{v}^{IV} = \bar{v}'' - \bar{u}'' = \bar{v}'' - \frac{\chi \bar{u}}{D} \overset{\circ}{\nabla}_\rho \bar{v}' \tag{12}$$

$$\bar{u}^{IV} = 3 \frac{(\bar{u}'')^2}{\bar{u}} + \left(1 - \frac{\chi \bar{u}}{D} \frac{\overset{\circ}{\nabla}_\rho \bar{u}'}{\bar{u}''} \right) \bar{u}'' \tag{13}$$

Notice that $\bar{u}'' < 0$. Hence we find that \bar{u} is a spike if

$$\frac{D}{\chi\bar{u}} < \frac{\overset{\circ}{\nabla}_\rho \bar{u}'}{\bar{u}''} < 1.$$

This can be satisfied if we know that $\bar{u} > \frac{D}{\chi}$ is large enough. Hence for $\bar{u} > \frac{D}{\chi}$ large enough we would expect spikes (although we cannot prove it here, since we need to compare $\overset{\circ}{\nabla}_\rho \bar{u}'$ with \bar{u}'').

For $\bar{u} > \frac{D}{\chi}$ we assume now that $v(\bar{x})$ is a plateau, i.e. $\bar{v}^{IV} < 0$. This implies that $\bar{v}'' < \frac{\chi\bar{u}}{D} \overset{\circ}{\nabla}_\rho \bar{v}'$ and with $\frac{\chi\bar{u}}{D} > 1$ this implies $\bar{v}'' < \overset{\circ}{\nabla}_\rho \bar{v}'$. If this last inequality is true for small ρ , then \bar{v} classifies as a spike, which contradicts the previous assumption. Hence \bar{v} cannot be a plateau.

A second argument can be obtained by expanding the non-local term up to $O(\rho^2)$:

$$\begin{aligned} u_t &= Du_{xxx} - \chi(uv_x + \frac{\rho^2}{3}uv_{xxx})_x \\ v_t &= v_{xx} + u - v \end{aligned}$$

At a local maximum (\bar{u}, \bar{v}) of the non-uniform steady state:

$$0 = D\bar{u}'' - \chi\bar{u}\bar{v}'' - \chi\frac{\rho^2}{3}\bar{u}\bar{v}^{IV} \quad (14)$$

$$0 = \bar{v}'' + \bar{u} - \bar{v} \quad (15)$$

Differentiation of (15) twice gives $\bar{v}'' = \bar{u}'' + \bar{v}^{IV}$, which we substitute into equation (14). After rearrangements we get

$$\bar{v}^{IV} = \frac{D - \chi\bar{u}}{D + \chi\bar{u}\frac{\rho^2}{3}}\bar{u}''$$

In the relevant region of parameter space for patterning, we have $\bar{u} > \frac{D}{\chi}$ and hence $\bar{v}^{IV} > 0$, i.e. \bar{v} is a spike. Note also that the above converges to the minimal case as $\rho \rightarrow 0$.

References

1. W. Allegretto, H. Xie, and S. Yang. Properties of solutions for a chemotaxis system. *J. Math. Biol.*, 35:949–966, 1997.
2. W. Alt. Biased random walk model for chemotaxis and related diffusion approximation. *J. Math. Biology*, 9:147–177, 1980.
3. W. Alt and D.A. Lauffenburger. Transient behavior of a chemotaxis system modelling certain types of tissue inflammation. *J. Math. Biol.*, 24(6):691–722, 1987.
4. M.D. Baker, P.M. Wolanin, and J.B. Stock. Signal transduction in bacterial chemotaxis. *Bioessays*, 28(1):9–22, 2006.
5. D Balding and D L McElwain. A mathematical model of tumour-induced capillary growth. *J Theor Biol*, 114(1):53–73, 1985.
6. P. Biler. Local and global solvability of some parabolic systems modelling chemotaxis. *Advances in Math. Sci. and Appl.*, 8(2):715–743, 1998.
7. P. Biler. Global solutions to some parabolic-elliptic systems of chemotaxis. *Adv. Math. Sci. Appl.*, 9(1):347–359, 1999.
8. J. P. Boon and B. Herpigny. Model for chemotactic bacterial bands. *Bull Math Biol*, 48(1):1–19, 1986.

9. C.J. Budd, R. Carretero-Gonzalez, and R.D. Russell. Precise computations of chemotactic collapse using moving mesh methods. *J. Comp. Phys.*, 202(2):463–487, 2005.
10. S.A. Budick and M.H. Dickinson. Free-flight responses of *Drosophila melanogaster* to attractive odors. *J. Exp. Biol.*, 209(Pt 15):3001–3017, 2006.
11. E.O. Budrene and H.C. Berg. Complex patterns formed by motile cells of *Escherichia coli*. *Nature*, 349(6310):630–633, 1991.
12. E.O. Budrene and H.C. Berg. Dynamics of formation of symmetrical patterns by chemotactic bacteria. *Nature*, 376(6535):49–53, 1995.
13. M. Burger, M. Di Francesco, and Y. Dolak-Struss. The Keller-Segel model for chemotaxis: linear vs. nonlinear diffusion. *SIAM J. Math. Anal.*, 2007. to appear.
14. H.M. Byrne, G. Cave, and D.L. McElwain. The effect of chemotaxis and chemokinesis on leukocyte locomotion: a new interpretation of experimental results. *IMA J. Math. Appl. Med. Biol.*, 15(3):235–256, 1998.
15. H.M. Byrne and M.R. Owen. A new interpretation of the keller-segel model based on multiphase modelling. *J. Math. Biol.*, 49:604–626, 2004.
16. M.A. Chaplain. Mathematical modelling of angiogenesis. *J. Neurooncol.*, 50(1-2):37–51, 2000.
17. M.A.J. Chaplain and A.M. Stuart. A model mechanism for the chemotactic response of endothelial cells to tumor angiogenesis factor. *IMA J. Math. Appl. Med. and Bio.*, 10:149–168, 1993.
18. S. Childress and J.K. Percus. Nonlinear aspects of chemotaxis. *Math. Biosci.*, 56:217–237, 1981.
19. J. Condeelis, R.H. Singer, and J.E. Segall. The great escape: when cancer cells hijack the genes for chemotaxis and motility. *Annu. Rev. Cell Dev. Biol.*, 21:695–718, 2005.
20. L. Corrias, B. Perthame, and H. Zaag. Global solutions of some chemotaxis and angiogenesis systems in high space dimensions. *Milan J. Math.*, 72:1–28, 2004.
21. F.W. Dahlquist, P. Lovely, and D.E. Koshland. Quantitative analysis of bacterial migration in chemotaxis. *Nature New Biol.*, 236:120–123, 1972.
22. J.C. Dallon and H.G. Othmer. A discrete cell model with adaptive signalling for aggregation of *dictyostelium discoideum*. *Philos. Trans. Roy. Soc. B*, 352:391–417, 1997.
23. F. Dkhil. Singular limit of a degenerate chemotaxis-fisher equation. *Hiroshima Math. J.*, 34:101–115, 2004.
24. Y. Dolak and T. Hillen. Cattaneo models for chemotaxis, numerical solution and pattern formation. *J. Math. Biol.*, 46(2):153–170, 2003.
25. Y. Dolak and C. Schmeiser. The Keller-Segel model with logistic sensitivity function and small diffusivity. *SIAM J. Appl. Math.*, 66:286–308, 2005.
26. D. Dormann and C.J. Weijer. Chemotactic cell movement during *Dictyostelium* development and gastrulation. *Curr. Opin. Genet. Dev.*, 16(4):367–373, 2006.
27. H.J. Eberl, D.F. Parker, and M.C.M. van Loosdrecht. A new deterministic spatio-temporal continuum model for biofilm development. *J. Theor. Medicine*, 3(3):161–175, 2001.
28. M. Eisenbach. *Chemotaxis*. Imperial College Press, London, 2004.
29. R.M. Ford and D.A. Lauffenburger. Measurement of bacterial random motility and chemotaxis coefficients: II. application of single cell based mathematical model. *Biotechnol. Bioeng.*, 37:661–672, 1991.
30. H. Gajewski and K. Zacharias. Global behavior of a reaction-diffusion system modelling chemotaxis. *Math. Nachr.*, 159:77–114, 1998.
31. S. Gueron and N. Liron. A model of herd grazing as a travelling wave, chemotaxis and stability. *J. Math. Biol.*, 27(5):595–608, 1989.
32. M. Henry, D. Hillhorst, and R. Schätzle. Convergence to a viscosity solution for an advection-reaction-diffusion equation arising from a chemotaxis-growth model. *Hiroshima Math. J.*, 29:591–630, 1999.

33. E. Hildebrand and U.B. Kaupp. Sperm chemotaxis: a primer. *Ann. NY. Acad. Sci.*, 1061:221–225, 2005.
34. T. Hillen. A classification of spikes and plateaus. *SIAM Reviews*, 49(1):35–51, 2007.
35. T. Hillen and H.G. Othmer. The diffusion limit of transport equations derived from velocity jump processes. *SIAM J. Appl. Math.*, 61(3):751–775, 2000.
36. T. Hillen and K. Painter. Global existence for a parabolic chemotaxis model with prevention of overcrowding. *Adv. Appl. Math.*, 26:280–301, 2001.
37. T. Hillen, K. Painter, and C. Schmeiser. Global existence for chemotaxis with finite sampling radius. *Discr. Cont. Dyn. Syst. B*, 7(1):125–144, 2007.
38. T. Höfer, J.A. Sherratt, and P.K. Maini. Dictyostelium discoideum: cellular self-organisation in an excitable biological medium. *Proc. R. Soc. Lond. B.*, 259:249–257, 1995.
39. D. Horstmann. Lyapunov functions and L^p -estimates for a class of reaction-diffusion systems. *Coll. Math.*, 87:113–127, 2001.
40. D. Horstmann. From 1970 until present: The Keller-Segel model in chemotaxis and its consequences I. *Jahresberichte der DMV*, 105(3):103–165, 2003.
41. D. Horstmann and A. Stevens. A constructive approach to traveling waves in chemotaxis. *J. Nonlin. Sci.*, 14(1):1–25, 2004.
42. E. Jabbarzadeh and C. F. Abrams. Chemotaxis and random motility in unsteady chemoattractant fields: a computational study. *J Theor Biol*, 235(2):221–232, 2005.
43. P. Kareiva and G. Odell. Swarms of predators exhibit 'prey-taxis' if individual predators use area-restricted search. *Am. Naturalist*, 130(2):233–270, 1987.
44. E.F. Keller and L.A. Segel. Initiation of slime mold aggregation viewed as an instability. *J. theo. Biology*, 26:399–415, 1970.
45. E.F. Keller and L.A. Segel. Model for chemotaxis. *J. Theor. Biology*, 30:225–234, 1971.
46. E.F. Keller and L.A. Segel. Traveling bands of chemotactic bacteria: A theoretical analysis. *J. Theor. Biol.*, 30:377–380, 1971.
47. J.S. Kennedy and D. Marsh. Pheromone-regulated anemotaxis in flying moths. *Science*, 184:999–1001, 1974.
48. I.C. Kim. Limits of chemotaxis growth model. *Nonlinear Analysis*, 46:817–834, 2001.
49. T. Kolokolnikov, T. Erneux, and J. Wei. Mesa-type patterns in the one-dimensional brusselator and their stability. *Physica D*, 214:63–77, 2006.
50. R. Kowalczyk. Preventing blow-up in a chemotaxis model. *J. Math. Anal. Appl.*, 305:566–588, 2005.
51. H. Kuiper. A priori bounds and global existence for a strongly coupled quasi-linear parabolic system modelling chemotaxis. *Electr. J. Diff. Eq.*, 52:1–18, 2001.
52. H. Kuiper and L. Dung. Global attractors for cross-diffusion systems on domains of arbitrary dimensions. *Rocky Mountain J. Math.*, 2007. to appear.
53. K.A. Landman, G.J. Pettet, and D.F. Newgreen. Chemotactic cellular migration: Smooth and discontinuous travelling wave solutions. *SIAM J. Appl. Math.*, 63(5):1666–1681, 2003.
54. K.A. Landman, G.J. Pettet, and D.F. Newgreen. Mathematical models of cell colonization of uniformly growing domains. *Bull. Math. Biol.*, 65(2):235–262, 2003.
55. I. R. Lapidus and R. Schiller. Model for the chemotactic response of a bacterial population. *Biophys J*, 16(7):779–789, 1976.
56. B. Larrivee and A. Karsan. Signaling pathways induced by vascular endothelial growth factor (review). *Int. J. Mol. Med.*, 5(5):447–456, 2000.
57. D A Lauffenburger and C R Kennedy. Localized bacterial infection in a distributed model for tissue inflammation. *J Math Biol*, 16(2):141–163, 1983.
58. J.M. Lee, T. Hillen, and M.A. Lewis. Continuous travelling waves for prey-taxis. *Bull. Math. Biol.*, 2007. in review.
59. H.A. Levine and B.D. Sleeman. A system of reaction diffusion equations arising in the theory of reinforced random walks. *SIAM J. Appl. Math.*,

- 57:683–730, 1997.
60. J.A. Logan, B.J. White, P. Bentz, and J.A. Powell. Model Analysis of Spatial Patterns in Mountain Pine Beetle Outbreaks. *Theor. Popul. Biol.*, 53(3):236–255, 1998.
 61. M. Luca, A. Chavez-Ross, L. Edelstein-Keshet, and A. Mogilner. Chemotactic signaling, microglia, and Alzheimer’s disease senile plaques: is there a connection? *Bull. Math. Biol.*, 65(4):693–730, 2003.
 62. P. K. Maini, M. R. Myerscough, K. H. Winters, and J. D. Murray. Bifurcating spatially heterogeneous solutions in a chemotaxis model for biological pattern generation. *Bull Math Biol*, 53(5):701–719, 1991.
 63. N.V. Mantzaris, S. Webb, and H.G. Othmer. Mathematical modeling of tumor-induced angiogenesis. *J. Math. Biol.*, 49(2):111–187, 2004.
 64. A. F. Maree and P. Hogeweg. How amoeboids self-organize into a fruiting body: multicellular coordination in *Dictyostelium discoideum*. *Proc Natl Acad Sci U S A*, 98(7):3879–3883, 2001.
 65. M. Mimura and T. Tsujikawa. Aggregation pattern dynamics in a chemotaxis model including growth. *Physica A*, 230:499–543, 1996.
 66. N. Mittal, E. O. Budrene, M. P. Brenner, and A. Van Oudenaarden. Motility of *Escherichia coli* cells in clusters formed by chemotactic aggregation. *Proc Natl Acad Sci U S A*, 100(23):13259–13263, 2003.
 67. I. Mori and Y. Ohshima. Molecular neurogenetics of chemotaxis and thymotaxis in the nematode *Caenorhabditis elegans*. *Bioessays*, 19(12):1055–1064, 1997.
 68. J.D. Murray. *Mathematical Biology II: Spatial models and biochemical applications*. Springer, New York, 3rd edition, 2003.
 69. J.D. Murray and M.R. Myerscough. Pigmentation pattern formation on snakes. *J. Theor. Biol.*, 149(3):339–360, 1991.
 70. M.R. Myerscough, P.K. Maini, and K.J. Painter. Pattern formation in a generalized chemotactic model. *Bull. Math. Biol.*, 60(1):1–26, 1998.
 71. T. Nagai, T. Senba, and K. Yoshida. Application of the Trudinger-Moser inequality to a parabolic system of chemotaxis. *Funkcialaj Ekvacioj*, 40(3):411–433, 1997.
 72. V. Nanjundiah. Chemotaxis, signal relaying and aggregation morphology. *J. Theoretical Biology*, 42:63–105, 1973.
 73. G.M. Odell and E.F. Keller. Traveling bands of chemotactic bacteria revisited. *J. Theor. Biol.*, 56(1):243–247, 1976.
 74. K. Osaki, T. Tsujikawa, A. Yagi, and M. Mimura. Exponential attractor for a chemotaxis-growth system of equations. *Nonlinear Analysis*, 51:119–144, 2002.
 75. K. Osaki and A. Yagi. Finite dimensional attractor for one-dimensional Keller-Segel equations. *Funkcialaj Ekvacioj*, 44:441–469, 2001.
 76. H.G. Othmer, S.R. Dunbar, and W. Alt. Models of dispersal in biological systems. *J. Math. Biol.*, 26:263–298, 1988.
 77. H.G. Othmer and T. Hillen. The diffusion limit of transport equations II: Chemotaxis equations. *SIAM J. Appl. Math.*, 62(4):1122–1250, 2002.
 78. H.G. Othmer and A. Stevens. Aggregation, blowup and collapse: The ABC’s of taxis in reinforced random walks. *SIAM J. Appl. Math.*, 57:1044–1081, 1997.
 79. M. R. Owen and J.A. Sherratt. Pattern formation and spatiotemporal irregularity in a model for macrophage-tumour interactions. *J. Theor. Biol.*, 189(1):63–80, 1997.
 80. K. Painter and T. Hillen. Volume-filling and quorum-sensing in models for chemosensitive movement. *Canadian Appl. Math. Quart.*, 10(4):501–543, 2002.
 81. K.J. Painter, P.K. Maini, and H.G. Othmer. Complex spatial patterns in a hybrid chemotaxis reaction-diffusion model. *J. Math. Biol.*, 41(4):285–314, 2000.
 82. K.J. Painter, P.K. Maini, and H.G. Othmer. Development and applications of a model for cellular response to multiple chemotactic cues. *J. Math. Biol.*,

-
- 41(4):285–314, 2000.
83. K.J. Painter, H.G. Othmer, and P.K. Maini. Stripe formation in juvenile poeciliids via chemotactic response to a reaction-diffusion mechanism. *Proc. Natl. Acad. Sci. USA*, 96:5549–5554, 1999.
 84. E. Palsson and H. G. Othmer. A model for individual and collective cell movement in *Dictyostelium discoideum*. *Proc Natl Acad Sci U S A*, 97(19):10448–10453, 2000.
 85. H.T. Park, J. Wu, and Y. Rao. Molecular control of neuronal migration. *Bioessays*, 24(9):821–827, 2002.
 86. C.S. Patlak. Random walk with persistence and external bias. *Bull. Math. Biophys.*, 15:311–338, 1953.
 87. B. Perthame. *Transport Equations in Biology*. Birkhäuser, 2007.
 88. A.J. Perumpanani, J.A. Sherratt, J. Norbury, and H.M. Byrne. Biological inferences from a mathematical model for malignant invasion. *Invasion Metastasis*, 16(4-5), 1996.
 89. K. Post. A non-linear parabolic system modeling chemotaxis with sensitivity functions, 1999.
 90. A. Potapov and T. Hillen. Metastability in chemotaxis models. *J. Dynamics Diff. Eq.*, 17:293–330, 2005.
 91. M. Rascole and C. Ziti. Finite time blow up in some models of chemotaxis. *J. Math. Biol.*, 33:388–414, 1995.
 92. M.A. Rivero, R.T. Tranquillo, H.M. Buettner, and D.A. Lauffenburger. Transport models for chemotactic cell populations based on individual cell behavior. *Chem. Eng. Sci.*, 44:1–17, 1989.
 93. L. A. Segel. Incorporation of receptor kinetics into a model for bacterial chemotaxis. *J Theor Biol*, 57(1):23–42, 1976.
 94. L.A. Segel. A theoretical study of receptor mechanisms in bacterial chemotaxis. *SIAM J. Appl. Math.*, 32:653–665, 1977.
 95. J.A. Sherratt. Chemotaxis and chemokinesis in eukaryotic cells: the Keller-Segel equations as an approximation to a detailed model. *Bull. Math. Biol.*, 56(1):129–146, 1994.
 96. J.A. Sherratt, E.H. Sage, and J.D. Murray. Chemical control of eukaryotic cell movement: a new model. *J. Theor. Biol.*, 162(1):23–40, 1993.
 97. A. Stevens. The derivation of chemotaxis-equations as limit dynamics of moderately interacting stochastic many particle systems. *SIAM J. Appl. Math.*, 61(1):183–212, 2000.
 98. T. Suzuki. *Free Energy and Self-Interacting Particles*. Birkhäuser, Boston, 2005.
 99. R. T. Tranquillo, D. A. Lauffenburger, and S. H. Zigmond. A stochastic model for leukocyte random motility and chemotaxis based on receptor binding fluctuations. *J Cell Biol*, 106(2):303–309, 1988.
 100. R. Tyson, S.R. Lubkin, and J.D. Murray. A minimal mechanism for bacterial pattern formation. *Proc. R. Soc. London B*, 266:299–304, 1999.
 101. R. Tyson, S.R. Lubkin, and J.D. Murray. Model and analysis of chemotactic bacterial patterns in a liquid medium. *J. Math. Biol.*, 38(4):359–375, Apr 1999.
 102. J.J.L. Velazquez. Point dynamics for a singular limit of the keller-segel model, I. motion of the concentration regions. *SIAM J. Appl. Math.*, 64(4):1198–1223, 2004.
 103. J.J.L. Velazquez. Point dynamics for a singular limit of the keller-segel model. II. formation of the concentration regions. *SIAM J. Appl. Math.*, 64(4), 2004.
 104. X. Wang. Qualitative behavior of solutions of chemotactic diffusion systems: Effects of motility and chemotaxis and dynamics. *SIAM J. Math. Ana.*, 31:535–560, 2000.
 105. Z. Wang and T. Hillen. Classical solutions and pattern formation for a volume filling chemotaxis model. *Chaos*, 17(037108), 2007. 13 pages.
 106. Z. Wang and T. Hillen. Shock formation in a chemotaxis model. *Math. Methods in the Appl. Sciences*, 31(1):45–70, 2008.

107. D.E. Woodward, R. Tyson, M.R. Myerscough, J.D. Murray, E.O. Budrene, and H.C. Berg. Spatio-temporal patterns generated by *Salmonella typhimurium*. *Biophys. J.*, 68(5):2181–2189, 1995.
108. D. Wrzosek. Long time behaviour of solutions to a chemotaxis model with volume filling effect. *Proc. Roy. Soc. Edinburgh Sect. A*, 136:431–444, 2006.
109. D. Wrzosek. Global attractor for a chemotaxis model with prevention of overcrowding. *Nonlin. Ana.*, 59:1293–1310, P2004.
110. D. Wu. Signaling mechanisms for regulation of chemotaxis. *Cell Res.*, 15(1):52–56, 2005.

Fig. 1 (M1) Numerical simulation of minimal model showing evolution of cell density (solid line) and chemical concentrations (dash-dot line) to the steady state. (M2)–(M8) Numerical results for the regularised models, showing steady state cell distributions (solid line) at different values of the regularisation parameter. For comparison, the steady state distribution of the minimal model is plotted as the dash-dotted line.

Fig. 1 (cont-d) The cell distributions marked with an asterisk have been classified (numerically) as plateau type – all others are spikes. For all numerics, the same model set-up is considered: parameters D and χ are set at 0.1 and 5.0 respectively; initial conditions are set to be $u(x, 0) = 1$ and $v(x, 0) = 1 + 0.1 \exp(-10x^2)$; 201 discretisation points are employed on a domain of length 1.

Fig. 2 Numerical simulations of models (M1)–(M8) on a larger domain from unbiased initial data. For all numerical simulations the following conditions are employed: parameters D and χ are set at 0.1 and 2.0 respectively; initial data $u(x, 0) = 1$ and $v(x, 0) = 1.0 + r(x)$ where $r(x)$ is a 1% random spatial perturbation of the steady state; domain $[0, 20]$ with 401 grid parameters.

Fig. 3 (a) 2-D numerical simulations showing cell density distributions from models (M1)–(M8). For model (M1) and (M2b) the solution is shown just prior to numerical blow-up. For models (M2a) and (M3)–(M8) the solution is shown following evolution to a steady state. (b) Evolution of the peak cell density on a logarithmic scale from the numerical simulations plotted in (a). In all numerical simulations the following conditions are employed: $D = 0.1$ and $\chi = 5.0$; initial data $u(x, y, 0) = 1$ and $v(x, 0) = 1 + 0.1 \exp(-10((x - 1)^2 + (y - 1)^2))$ on the unit square.

Fig. 4 (a) Numerical simulation of the 2-D model for chemotaxis incorporating receptor binding (with $\alpha = 0.5$), volume-filling ($\gamma = 10$), non-linear diffusion ($n = 1.0$) and saturating chemical production ($\phi = 1.0$). (b) As for (a), but with the addition of logistic cell growth ($r = 0.1$). For both sets of numerics we let $D = 0.1$, $\chi = 5.0$ on a domain of size 20×20 with initial data $u(x, y, 0) = 1$ and $v(x, y, 0) = 1.0 + r(x, y)$, where $r(x, y)$ is a 1% random spatial perturbation of the steady state.

Fig. 5 Numerical simulation of the volume filling model (M4a) in 3D. Left hand plots show cell density distribution at various “slices” through the 3D data, right hand plots shows the contours for which $u = 5$. (a) Formation of a spherical aggregation of cells from biased initial conditions, $u(x, y, z, 0) = 1$ and $v(x, y, z, 0) = 1 + 0.1 \exp(-10((x - 1)^2 + (y - 1)^2 + (z - 1)^2))$ on the $2 \times 2 \times 2$ -cube. (b) Pattern formed from random initial data on a larger domain at $t = 100.0$. In both simulations we set $D = 0.1$, $\chi = 5.0$ and $\gamma = 10$ and employ $41 \times 41 \times 41$ spatial grid points.